In-Situ Thermal Imaging for Quality Classification of Dissimilar Metal Laser Welds in Battery Tab Welding

Thienan Hoang[a], Mumin Adhami[a], Mateo E. Garcia-Sandoval[a], Can Sun[a], Austin R.J. Downey[a,b], Yanzhou Fu[c], Lang Yuan[a], and Cebastione Bailey[a]

[a]Department of Mechanical Engineering, University of South Carolina, Columbia, USA
[b]Department of Civil and Environmental Engineering, University of South Carolina, Columbia, USA
[c]Department of Ocean and Mechanical Engineering, Florida Atlantic University, Boca Raton, FL, USA

ABSTRACT

Battery tab welding is critical for the optimal performance and long-term reliability of lithium-ion battery packs. Inadequate weld quality can reduce battery efficiency, lower thermal performance, and introduce safety risks, including the potential for thermal runaway. Poor welds also increase manufacturing costs related to scrap and rework. As demand for advanced battery systems in electric vehicles, consumer electronics, and energy storage continues to grow, there is an urgent need to improve the reliability and consistency of battery tab welding. Traditional quality assurance methods, such as X-ray imaging, ultrasonic inspection, and destructive testing, verify safety standards but are performed ex-situ and on a sampling basis, often testing only every hundredth cell or pack. These approaches are time-consuming and cannot detect defective welds in real time. To address these challenges, a custom platform that integrates a thermal camera into a laser welding setup was developed. Thermal imaging records spatial and temporal temperature distributions, peak temperatures, and cooling rates across the weld region. Key features are extracted from the thermal data using computer vision techniques, enabling correlation of thermal behavior, including hotspot persistence, thermal gradients, and cooling dynamics, with weld quality indicators such as porosity, lack of fusion, and overheating. Experimental results demonstrate a weld success rate of 70%, with thermal features enabling clear differentiation between successful and failed welds. These findings highlight the potential of in-situ monitoring for real-time process control in battery manufacturing.

Keywords: Batteries, Laser welding, in-situ monitoring

1. INTRODUCTION

Battery tab welding is a critical process in lithium-ion battery manufacturing, directly influencing electrical efficiency, thermal behavior, and mechanical integrity.[1] Variations in laser welding parameters such as power, speed, and focal position can significantly affect melt pool dynamics, leading to defects including porosity, lack of fusion, and burn-through. These defects increase electrical resistance, degrade mechanical performance, and, in severe cases, introduce safety risks such as thermal runaway.[2] Ensuring consistent, high-quality welds is therefore essential for reliable and cost-effective battery production.

Conventional quality assurance methods are primarily conducted ex-situ using techniques such as X-ray imaging and ultrasonic testing[3,4]. While effective for defect characterization, these approaches are typically applied on a sampling basis and do not provide real-time feedback. As a result, defects may only be detected after large production batches have already been completed, limiting process control and increasing scrap and rework.

Further author information: (Send correspondence to Austin Downey)
Austin Downey: Email: austindowney@sc.edu

To address these limitations, in-situ monitoring approaches have been explored to capture process signatures during welding.[5] Optical imaging provides information on melt pool geometry and spatter, while thermal imaging captures temperature evolution and cooling behavior[6,7]. These signatures are directly linked to weld formation mechanisms and offer the potential for real-time defect detection. However, many existing approaches focus on geometric features or single-sensor measurements, with limited correlation to mechanical performance.

This work presents an in-situ thermal monitoring approach for battery tab welding by integrating a thermal imaging system within a custom enclosure to capture spatial and temporal temperature distributions. Laser speed is systematically varied to establish relationships between energy input, thermal response, and weld integrity. Tensile shear testing validates the predictive capability of thermal features, demonstrating that in-situ thermal data can distinguish between underscanned, optimal, and overscanned welding conditions. These results support the development of a high-throughput cell to pack battery manufacturing framework with real-time cell/tab weld quality monitoring. The contributions of this study are twofold: (1) demonstrating the feasibility of in-situ thermal monitoring for battery tab welding, and (2) establishing a machine learning pipeline for real-time weld quality classification based on thermal features. Data associated with this paper are available in a public repository;[8] the specific data used in this study are labeled *Dataset-1*.

The rest of the paper is structured as follows: Section 2 describes the experimental setup, Section 3 presents the results, and Section 4 concludes the paper.

2. METHODOLOGY

2.1 Test Setup

The driving motivation for this work is high-throughput battery manufacturing, with a focus on laser welding of battery tabs. While the long-term vision includes integration into advanced battery pack architectures, such as the Smart Pack for Advanced Research and Control (SPARC)[9] shown in Figure 1(a), the present study focuses specifically on tab-level welding. Although the specimens used here are not full batteries, they are designed to replicate key material and structural features relevant to battery cell/tab welding.

The weld specimens consisted of a 0.15 × 8 × 100 mm strip of nickel-plated steel temporarily fixed using high-temperature tape to a strip of stainless steel with nominal dimensions of 0.6 × 9.65 × 85 mm cut from larger sheet stock. The material pairing was selected to approximate commercially relevant battery tab-to-case configurations, with nickel tabs and stainless steel casings representative of cylindrical cells (e.g., Samsung 30Q). The nickel strip was laser-welded to the stainless steel strip. One sample was placed in a jig consisting of a steel block clamped to an aluminum breadboard plate with a threaded hole array. The specimen was clamped

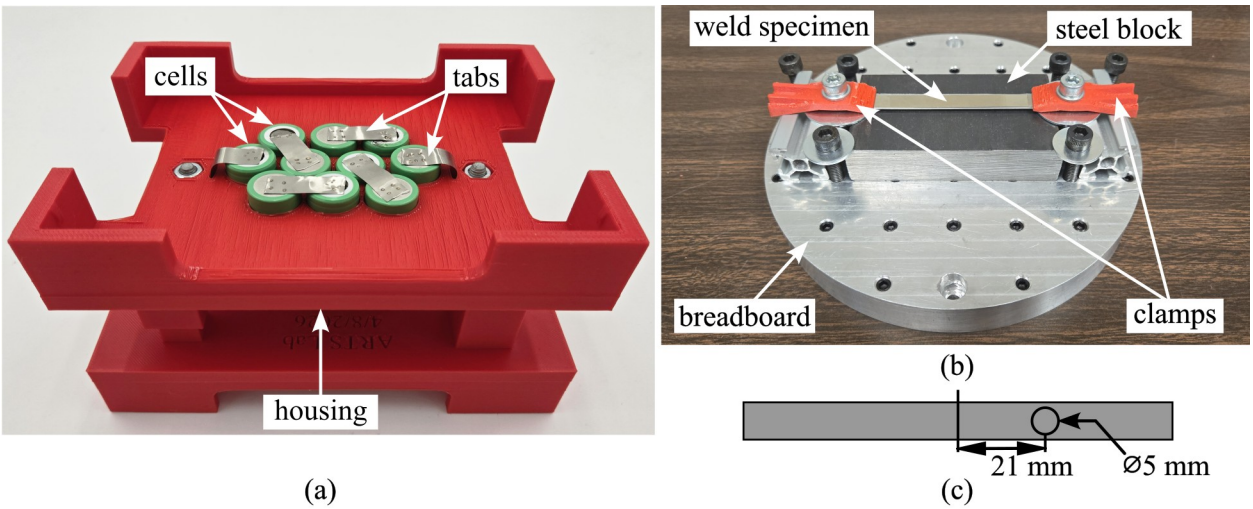

Figure 1: Test hardware setup, showing: (a) a custom housing for 18650 batteries with welded tabs; (b) the test jig holding one weld specimen; and; (c) a diagram of the weld pattern for all specimens.

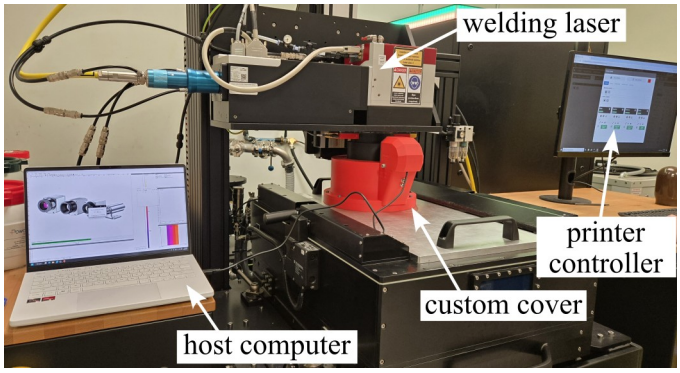

Figure 2: Custom cover equipped with a thermal camera, host computer, and welding equipment.

Table 1: Laser weld parameters.

Test	Spot Size	Speed	Power
1	150 µm	45 mm/s	300 W
2	150 µm	45 mm/s	300 W
3	150 µm	60 mm/s	300 W
4	150 µm	60 mm/s	300 W
5	150 µm	75 mm/s	300 W
6	150 µm	75 mm/s	300 W
7	150 µm	90 mm/s	300 W
8	150 µm	90 mm/s	300 W
9	150 µm	105 mm/s	300 W
10	150 µm	105 mm/s	300 W

between a custom 3D printed clamp made from glass-filled ABS and a steel spacer washer to maintain a fixed gap between the specimen and the steel block as seen in Figure 1(b). The gap was introduced to mimic the structure seen between a terminal and the current interruption device in an 18650 battery. This gap remains constant throughout all tests. The jig assembly was mounted inside the build chamber of an Aconity MIDI laser powder bed fusion system.

A custom cover for the printer (Figure 2) was designed and fabricated to house a thermal camera equipped with a built-in 18° × 14° field-of-view lens; as discussed in Adhami et al.[10] The structural components were manufactured using glass-filled ABS via 3D printing. The housing section also features a 240 mm diameter fused silica optical window with a 1040 nm anti-reflective coating, allowing the build chamber to operate under an argon atmosphere. For this experiment, the glass was removed to allow accurate temperature values to be recorded. The cover features locking magnets that mate with the printer head, providing a safety interlock and secure attachment during operation.

2.2 Laser Welding

Laser welding was performed with laser speed as an independent variable. The corresponding parameter values are provided in Table 1. Power and spot size remained constant throughout all test runs. Two specimens were welded at each power level. The build chamber was not filled with argon during any test run, and welding was conducted under ambient atmospheric conditions.

Each specimen was welded with a circular pattern (dimensions shown in Figure 1(c)), and thermal footage was captured during laser exposure. Each weld consisted of a single-pass circular scan with a diameter of 5 mm to accommodate the strip size. A circular pattern was selected to avoid stress concentrations seen in shapes with angled vertices. After each test run, the specimen was removed and replaced. Alignment of the specimen was performed manually using an onboard guide laser. Results recorded during this procedure included thermal imaging data and binary success verification via visual inspection and a shim to confirm weld contact.

(a) (b)

Figure 3: Testing configuration, showing: (a) the MTS Exceed E43 tensile tester in use; and; (b) all test specimens.

Table 2: Summary of weld joint outcomes. Failure mode is reported as "weld", "nickel strip", "both", or "n/a" if the weld was unsuccessful.

Test	Failure location
1	nickel strip
2	nickel strip
3	n/a
4	nickel strip
5	nickel strip
6	weld
7	nickel strip
8	nickel strip
9	n/a
10	both

2.3 Tensile Test

Tensile testing of the specimens was performed using an MTS Exceed E43 electromechanical universal test system (Figure 3(a)). Specimens that passed preliminary inspection after welding were then placed in the tester with the nickel strip clamped in the upper jaw and the stainless steel strip in the lower jaw. The load was applied parallel to the weld plane. Parameters for the tensile test were a cross-head speed of 0.0762 mm/s (0.003 in/s) and a data acquisition rate of 10.0 Hz. A 17.8 kN (4000 lbf) preload was applied to the machine to eliminate errors during testing. Specimens were inserted at a consistent depth within the jaws to ensure repeatable alignment and minimize bending. Data collected during this procedure included peak load, failure mode, force-displacement curves, and whether failure occurred in the nickel strip, at the weld interface, or both.

3. RESULTS

Table 2 summarizes the binary pass/fail outcomes, while Figure 3(b) presents representative weld morphologies. The welds achieved a success rate of 70% in weld performance after the welding process. All successful welds exhibited failure in the nickel strip rather than at the weld interface, suggesting that the weld strength exceeded the tensile strength of the base material. This behavior is indicative of a mechanically robust joint.

Thermal images were generated from cropped regions of interest to focus specifically on the weld zone. Frame selection was performed using a systematic and objective method: for each weld, the frame corresponding to the highest peak pixel intensity was identified and used for analysis. Selecting the maximum-intensity frame ensures that the image represents the moment of greatest thermal input and melt pool development, providing a consistent basis for comparison across specimens.

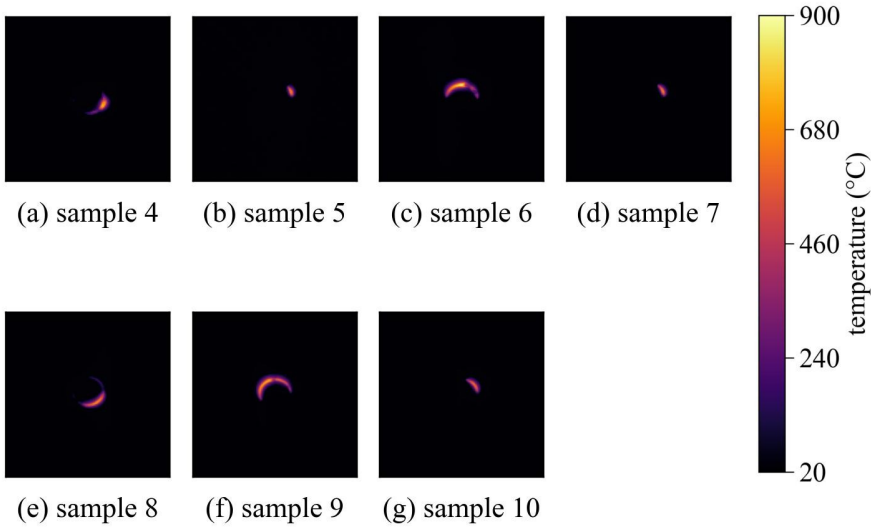

Figure 4: Representative thermal images comparing unsuccessful and successful welds.

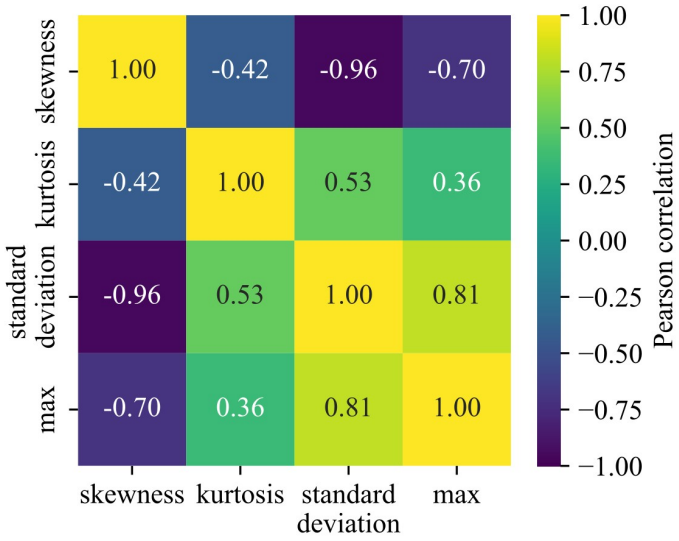

Figure 5: Pearson correlation matrix used to find features that are independent from the others.

Welds that featured darker fusion rings with large heat tinting led to failed welds or failure at the weld interface during tensile testing. Conversely, welds that featured relatively thin, discrete fusion rings tended to have the nickel strip fail during tensile testing. This is supported by thermal footage (Figure 4), which shows unsuccessful welds having larger heat signatures than the successful welds seen in (Figure 3(b)). Additionally, heat persists longer for unsuccessful welds, while successful welds cool almost immediately.

After extracting the frames, a set of statistical features was computed over each entire frame. A correlation matrix was then generated to identify the most independent features. Based on this analysis (Figure 5), skewness, standard deviation, maximum value, and kurtosis were selected as the most independent features. Two-dimensional logistic regression decision boundaries[11] were then computed for each pair of features, as shown in Figure 6.

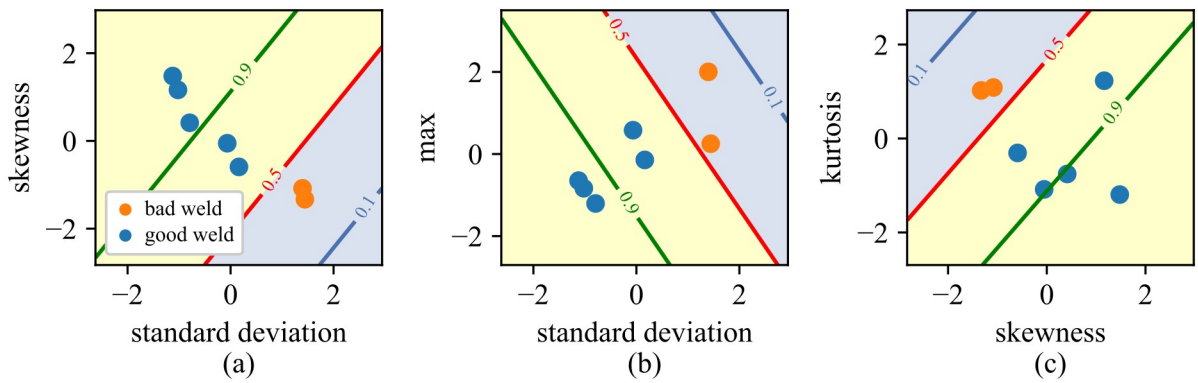

Figure 6: Boundary plots marking good and bad welds.

A source of weld failure beyond process parameters may be clamp compliance during tightening, which can cause the nickel strip to bow inward. This deformation may reduce thermal contact with the stainless steel substrate, limiting heat dissipation and resulting in the larger heat signatures observed in Figure 4. This effect could be mitigated by using stiffer clamping fixtures.

4. CONCLUSION

This work demonstrates the feasibility of in-situ thermal monitoring for battery tab weld quality classification using features extracted directly from thermal image data. Statistical features, such as skewness, standard deviation, and kurtosis, effectively capture differences in melt pool behavior and heat distribution associated with weld formation, enabling discrimination between successful and failed welds. Experimental results show a weld success rate of 70%. Experimental results show that welds exhibiting smaller, rapidly dissipating thermal signatures tend to produce stronger joints, while larger, persistent heat signatures are associated with defects and weaker weld performance. Two-dimensional logistic regression decision boundaries further confirm that these features provide meaningful class separation. These findings suggest that thermal imaging can serve as a non-destructive, real-time monitoring tool capable of evaluating weld quality on a weld-by-weld basis. Future work will expand the dataset, investigate feature importance and univariate models, and explore integration of thermal-based classification into real-time process monitoring and control frameworks for improved consistency and reliability in battery manufacturing.

5. ACKNOWLEDGMENTS

This research was supported by the United States' National Science Foundation (NSF), Grants Nos. CCF-2503055, and CPS-2237696. This work is also partially supported by the National Institute of Standards & Technology, United States, under grant number 70NANB23H030, as well as the South Carolina Space Grant Consortium under grants 25-073-BTC-SC-001, 25-073-REAP-SC-001, and 25-073-REAP-SC-003. Additional support is provided by the United States' National Science Foundation (NSF) through the NSF ASEE Fellowship. Any opinions, findings, conclusions, or recommendations expressed in this material are those of the authors and do not necessarily reflect the views of the National Science Foundation, the South Carolina Space Grant Consortium, or the National Institute of Standards & Technology.

REFERENCES

1. Rapp, S., *Optimising tab welding in lithium-ion battery manufacturing: on the advantages of laser welding over ultrasonic welding*, Master's thesis, KTH, Production engineering (2024).
2. Yao, X.-Y. and Pecht, M. G., "Tab design and failures in cylindrical Li-ion batteries," *IEEE Access* **7**, 24082–24095 (2019).

3. Wang, Y., Lai, X., Chen, Q., Han, X., Lu, L., Ouyang, M., and Zheng, Y., "Progress and challenges in ultrasonic technology for state estimation and defect detection of lithium-ion batteries," *Energy Storage Materials* **69**, 103430 (May 2024).
4. Masuch, S., Gümbel, P., Kaden, N., and Dröder, K., "Applications and development of X-ray inspection techniques in battery cell production," *Processes* **11**, 10 (Dec. 2022).
5. Gester, A., Tetzner, A., Wagner, G., Gluchowski, P., Becker, M., Deutsch, M., and Leoka, D., "Development of a process monitoring method for ultrasonic metal welding of automotive wires based only on machine sensor data," *Welding in the World* **70**, 1123–1144 (Jan. 2026).
6. Li, X., Li, H., Chen, X., Shen, S., Zhang, G., Wei, H., Hu, Y., Li, Z., and Dai, L., "In-situ multi-eye monitoring of melt pool temperature field in laser additive manufacturing by light field camera," *Additive Manufacturing* **102**, 104747 (Mar. 2025).
7. Era, I. Z., Zhou, F., Raihan, A. S., Ahmed, I., Abul-Haj, A., Craig, J., Das, S., and Liu, Z., "In-situ melt pool characterization via thermal imaging for defect detection in directed energy deposition using vision transformers," *Journal of Manufacturing Processes* **145**, 11–21 (July 2025).
8. ARTS-Lab, "Arts-laboratory/dataset-battery-tab-laser-welding." GitHub. https://github.com/ARTS-Laboratory/ARTS-Laboratory/Dataset-battery-tab-laser-welding, , accessed April 18, 2026.
9. ARTS-Lab, "Smart-pack-for-advanced-research-and-control." GitHub. https://github.com/ARTS-Laboratory/Smart-Pack-for-Advanced-Research-and-Control, accessed April 18, 2026.
10. Adhami, M., Garcia-Sandoval, M., Hoang, T., Whetham, M., Sun, C., Downey, A. R. J., Fu, Y., and Yuan, L., "Design of vacuum- and pressure-compatible optical and thermal camera modules for laser powder bed fusion," in [*Nondestructive Characterization and Monitoring of Advanced Materials, Aerospace, Civil Infrastructure, and Transportation XX*], Wu, H. F., ed., 16, SPIE (Apr. 2026).
11. Downey, A., "Machine learning for engineering problem solving: A practical example-driven guide to classical techniques," (2025).